Acta Crystallographica Section B
**Structural Science**
ISSN 0108-7681

# Structure of $\delta_1$-$CoZn_{7.8}$, an example of a phason pinning–unpinning transformation?

**Hanna Lind,[a]* Magnus Boström,[b] Vaclav Petříček[c] and Sven Lidin[a]**

[a]Department of Inorganic Chemistry, Stockholm University, 10691 Stockholm, Sweden, [b]Department of Structural Chemistry, Stockholm University, 10691 Stockholm, Sweden, and [c]Institute of Physics, Academy of Sciences of the Czech Republic, Na Slovance 2, 180 40 Praha 8, Czech Republic

Correspondence e-mail: hanna@inorg.su.se

Received 11 June 2003
Accepted 8 September 2003

The novel structure of the $\delta_1$ phase in the cobalt–zinc system was determined by single-crystal X-ray diffraction. The structure features fused double icosahedra linked by edge- and face-sharing. The $\delta_1$-$CoZn_{7.8}$ structure is incommensurately modulated along the columnar $b$ direction. The extent of the linear pentagonal antiprismatic intergrowth is limited to a maximum of two overlapping icosahedra because of geometric demands and radii relations. Even this limited fusion of icosahedra leads to strain that is believed to be the origin of the structural modulation. The compound was synthesized using a centrifugation-aided filtration method which yielded single crystals grown on cobalt pieces in a zinc-rich melt. The $(3 + 1)$-dimensional superspace group is $F2/m(0\beta0)s0$ and the modulation wavevector was determined to $\mathbf{q} = 0.234\mathbf{b}^*$. The partial amorphization of the sample when subjected to mechanical grinding is an indication of a metastable structure. The incommensurability of the structure may be seen as an ordered pinning of phasons.

## 1. Introduction

A survey of zinc-rich intermetallic compounds demonstrates a strong tendency for zinc to form structures with icosahedral assemblies. The organization of this prevalent structural element varies in these compounds, from isolated icosahedra stabilized by bridging atoms (as in $NaZn_{13}$) and interconnected icosahedra in different forms [as in *e.g.* $TiZn_6$, $Ni_3Zn22$ and $\gamma$-brass ($Cu_5Zn_8$)] to local icosahedral symmetries, as in quasicrystals [*e.g.* in the Zn–Mg–(Y, RE) systems (RE = rare earth metal)]. The zinc-rich compounds of the cobalt–zinc system are no exception given that the previously known structures of Γ, $\delta$ and $\zeta$ can all be described as built from icosahedra. The Γ-$Co_5Zn_{21}$ structure (Ekman, 1931) belongs to the $\gamma$-brass class of compounds and involves face-sharing icosahedra, forming tetrahedral clusters that are interconnected *via* vertex-sharing. The recently reported structure of $\delta$-$Co_2Zn_{13}$ (Boström & Lidin, 2002) can be described either as vertex-sharing or as composed of face-sharing icosahedra, forming a double helix along the $c$ axis. The most zinc-rich phase, the monoclinic $\zeta$-$CoZn_{13}$ (Brown, 1962), exhibits vertex-sharing icosahedra.

The zinc-rich $\delta_1$ phase in the Co–Zn system was first reported by Schramm (1938*a*).[1] Schramm (1938*b*) observed that the powder X-ray diffraction pattern showed similarities

[1] This phase is designated '$\gamma_1$' in *Binary Alloy Phase Diagrams* (Massalski, 1990).

with that of $\gamma$-brass and suggested the $\delta_1$ phase has a distorted $\gamma$-brass structure.

It is noteworthy that single icosahedra constitute the building blocks of a large number of structure types of metal compounds. However, extended forms of icosahedral packing, with linear sequences of fused icosahedra, are far less common. Up to now, no known example exists in the structurally rich zinc chemistry and fewer than a dozen cases occur in all of inorganic chemistry.

We present here the full structure of incommensurately modulated $\delta_1$-$CoZn_{7.8}$, a novel structure with extended icosahedral packing, solved from single-crystal X-ray diffraction data. The pentagonal antiprismatic columns in the $\delta_1$-$CoZn_{7.8}$ structure are limited to fused double icosahedra; that limitation can be shown to be a consequence of simple geometrical constraints. This will be discussed and compared with other compounds built by pentagonal antiprismatic columns.

## 2. Experimental

The synthesis was carried out using the centrifugation-aided filtration method of Boström & Hovmöller (2000). Using this method, single crystals were grown on the high melting reactant (Co) in a melt rich in the low melting reactant (Zn), which acted as a self-flux. According to the cobalt–zinc binary phase diagram by Schramm (1938*a*), a two-phase area ($\delta_1 + l$) exists at > 89 at.% Zn in the temperature range 839–948 K. A synthesis in this area will produce crystals with the composition of the solidus line, solely dependent on the reaction temperature.

Zinc pellets (2.14 g, Kebo, 99.9%) and cobalt powder (0.095 g, ABCR, 99.9%) were pressed to a pellet and placed in an evacuated quartz ampoule containing a fixed filter of quartz wool on a support of crushed quartz glass in one end of the ampoule and the reactants in the other end. The ampoule was kept with the filter end upwards in an insulated container in a furnace at 873 K for 40 h and then turned upside down in a centrifuge where the melt was removed by centrifugal filtration. Tabular single crystals with a silvery lustre in up to millimetre sizes were found on top of the filter after the centrifugation. The crystals were of high quality for single-crystal X-ray diffraction purposes, although very brittle. Powder X-ray diffraction data was collected on a GUINIER-HÄGG camera with Cu $K\alpha_1$ radiation. Owing to the small amount of cobalt in the sample (approximately 11 at.%), fluorescence was not a problem.

The approximate composition was determined from EDX analyses on several crystals.

The single-crystal X-ray data was collected on a Stoe imaging plate-detector system (IPDS) mounted on a Siemens rotating-anode X-ray source producing Mo $K\alpha$ radiation. Data reduction and a numerical absorption correction was applied to the data using the *XRED* (Stoe & Cie, 1996*a*) and *XSHAPE* (Stoe & Cie, 1996*b*) programs. The structure was partially solved using direct methods with *SHELXS*97 (Sheldrick, 1997) and the program package *JANA*2000 (Petříček & Dušek, 2000) was used for the structure refinements.

**Table 1**
Experimental table.

| | |
|---|---|
| Crystal data | |
| Chemical formula | $CoZn_{7.8}$ |
| $M_r$ | 568.90 |
| Cell setting, space group | Monoclinic, $F2/m(00\gamma)s0$ |
| $a, b, c$ (Å) | 9.030 (2), 4.3380 (10), 12.511 (3) |
| $\beta$ (°) | 89.90 (3) |
| $V$ (Å$^3$) | 490.1 (2) |
| $Z$ | 2 |
| $D_x$ (Mg m$^{-3}$) | 3.854 (2) |
| Radiation type | Mo $K\alpha$ |
| No. of reflections for cell parameters | 2026 |
| $\theta$ range (°) | 2.9–48.4 |
| $\mu$ (mm$^{-1}$) | 20.29 |
| Temperature (K) | 293 |
| Crystal form, colour | Tabular, metallic |
| Crystal size (mm) | 0.08 × 0.05 × 0.02 |
| **q** | 0.234**b*** |
| Data collection | |
| Diffractometer | Stoe IPDS |
| No. of images | 250 |
| Data collection method | $\theta$–$2\theta$ |
| Absorption correction | Numerical from crystal shape |
| $T_{min}$ | 0.263 |
| $T_{max}$ | 0.724 |
| No. of measured, independent and observed reflections | 8488, 2026, 1095 |
| No. of main reflections | 734 |
| No. of satellites | 7754 |
| No. of unique main reflections | 198 |
| No. of unique satellites | 1470 |
| Criterion for observed reflections | $I > 3\sigma(I)$ |
| $R_{int}$ | 0.075 |
| $\theta_{max}$ (°) | 48.4 |
| Range of $h, k, l$ | $-10 \Rightarrow h \Rightarrow 10$<br>$0 \Rightarrow k \Rightarrow 5$<br>$0 \Rightarrow l \Rightarrow 14$ |
| Refinement | |
| Refinement on | $F$ |
| $R[F^2 > 2\sigma(F^2)]$, $wR(F^2)$, $S$ | 0.062, 0.069, 2.92 |
| $R_{main}$ | 0.0416 |
| $R_{satellites}$, first-order | 0.0521 |
| Second order | 0.0641 |
| Third order | 0.1039 |
| Fourth order | 0.2110 |
| No. of relections | 2026 |
| No. of parameters | 104 |
| Weighting scheme | Based on measured s.u.'s<br>$w = 1/[\sigma^2(F) + 0.0001F^2]$ |
| $(\Delta/\sigma)_{max}$ | <0.0001 |
| $\Delta\rho_{max}$, $\Delta\rho_{min}$ (e Å$^{-3}$) | 4.98, −4.53 |

Computer programs used: *XRED* (Stoe & Cie, 1996*a*), *JANA*2000 (Petříček & Dušek, 2000).

## 3. Results

The composition of the phase was, according to the EDX analysis, established to 88.6 ± 0.3 at.% Zn, or approximately $CoZn_{7.8\ (3)}$.

**Table 2**
Atomic data for the average cell.

| | Wyckoff position | $x$ | $y$ | $z$ | $U_{eq}$ |
|---|---|---|---|---|---|
| Co | 16(*j*) | −0.1608 (2) | −0.3052 (4) | 0.0879 (2) | 0.0105 (4) |
| Zn1 | 8(*i*) | −0.2128 (2) | 0 | 0.09149 (9) | 0.0173 (3) |
| Zn2 | 8(*i*) | 0.4160 (2) | 0 | 0.0215 (2) | 0.0214 (5) |
| Zn3 | 8(*i*) | 0.2705 (2) | 0 | 0.2311 (2) | 0.0136 (4) |
| Zn4 | 8(*i*) | 0.07311 (9) | 0 | 0.09012 (7) | 0.0145 (3) |
| Zn5 | 8(*i*) | −0.43014 (9) | 0 | 0.21472 (7) | 0.0139 (3) |

**Table 3**
Special function parameters.

| | | | |
|---|---|---|---|
| Co | Amplitude $u_y$ = 0.01 (2) | $x_4^0$ = 0.161 (6) | $\Delta$ = 0.241 (1) |
| Zn1 | Amplitude $u_y$ = 0.082 (7) | $x_4^0$ = 0.75 | $\Delta$ = 0.759 (1) |
| Zn2 | $x_4^0$ = 0.75 | $\Delta$ = 0.5 | |
| Zn3 | $x_4^0$ = 0.75 | $\Delta$ = 0.5 | |

### 3.1. Single-crystal X-ray diffraction

The single-crystal diffraction pattern showed strong main reflections and additional incommensurate satellite reflections.

The diffraction data proved to be metrically orthorhombic and the lattice clearly F-centred, but no further systematic extinctions could be observed. The basic cell dimensions are given in Table 1.[2] The satellite reflections could all be indexed using one modulation vector, **q**, parallel to **b***, **q** = $\beta$[010]*. The determination of $\beta$ was chosen so that the distribution of the satellite reflections showed declining intensities with satellite order. Satellites of up to the fifth order were detected within the criterion for observation [$I \geq 3\sigma(I)$]. The value of $\beta$ is approximately equal to 0.234 and although this value is close to the rational number 4/17, it is clear from precession photographs that **q** qualitatively differs from commensurability. The numerical accuracy of $\beta$ cannot be established with the imaging-plate-detector system used in the measurement.

The solution of the average structure was first attempted in the space group *Fmmm*, but after several failed attempts with possible orthorhombic space groups, the symmetry was lowered and the crystal class was changed to monoclinic. This change was supported by the internal $R$ values, which for all main reflections after averaging in the orthorhombic space groups were all above 0.25 but dropped to 0.063 when the space group was altered to F2/*m*. This non-conventional space group (conventional setting *C*2/*m*, No. 12) gave satisfactory $R$ values for the average structure and the 734 main reflections. In an axial monoclinic system (a monoclinic lattice of main reflections with a modulation vector running along the unique axis) with the basic space group *F*2/*m*, the only possible super space groups are *F*2/*m*(0$\beta$0) and *F*2/*m*(0$\beta$0)*s*0, non-conventional setting. The latter requires the special reflection condition of *0k0m*: *m* = 2*n*, which was fulfilled by the large satellite reflection material and hence the superspace group used in the refinements was *F*2/*m*(0$\beta$0)*s*0. The final convergence to low $R$ values proved this conclusion to be right. All experimental details can be found in Table 1.

The standard choice of superspace group is, according to the *International Tables of Crystallography* (1995, Vol. C), *B*2/*m*(00$\gamma$)*s*0, but the non-conventional F-centred cell was chosen in order to preserve the metrically orthorhombic cell.

The structure solution and subsequent refinements yielded six atomic positions, five with eightfold multiplicity [Wyckoff position 8(*i*)] and one with 16-fold multiplicity [Wyckoff position 16(*j*)]. The site with the highest multiplicity was assumed to be cobalt based on the icosahedral coordination of cobalt that seems to be characteristic not only of zinc-rich cobalt–zinc compounds, but of compounds in general with zinc and transition metals. Table 2 gives the details of the average cell parameters and isotropic temperature factors for the atoms.

Atomic modulation functions (AMFs) were applied to all atoms. The displacements of the Zn1 and Co atoms in the *b* direction were modelled with a combination of harmonic functions and a sawtooth function characterized by its centre $x_4^0$, its width $\Delta$ and a maximal displacement $\mathbf{u}_0$ from the average position. The sawtooth function describes both the positional displacement of an atom and the restricted interval where the same atom exists. The occupation of cobalt ($\Delta_{Co}$) is hence limited by $\Delta_{Co} = 1 - \Delta_{Zn}$ ($\Delta_{Co}$ = width of the sawtooth function for Co, $\Delta_{Zn}$ = width of the sawtooth function for Zn1). During refinements, $\Delta_{Co}$ was fixed to the composition determined from EDX. A non-restricted $\Delta_{Co}$ led to an indistinguishable result.

Two other zinc positions (Zn2 and Zn3) were modelled with positional displacement waves on an interval defined by a crenel function (Petříček *et al.*, 1995) and the last two zinc positions (Zn4 and Zn5) were modelled with positional displacement waves. Modulation waves of thermal displacement parameters were applied to three zinc atoms (Zn1, Zn4 and Zn5). Generally, the AMFs were chosen on the basis of the appearance of each atom in $F_{obs}$. See Table 3 for the special function parameters and Table 4 for all modulation function coefficients.

The use of special functions such as *e.g.* crenel functions and sawtooth functions has the advantage that highly anharmonic behaviour may be accurately modelled using a significantly lower number of parameters. The special functions are often used together with harmonic modulation functions, with the intention of softening the shape of the special function. The combination of a harmonic function and a discontinuous function (or a function with discontinuous derivatives) has the disadvantage that the orthogonality condition is not fulfilled for the harmonic functions. This may create refinement problems, such as strong correlations between positional or thermal displacement parameters. To avoid correlations, an orthogonalization of the basic functions is made, which transforms the total set of basic functions to a new complete set of orthogonalized functions (Petříček *et al.*, 1995). The method is based on the Schmidt orthogonalization procedure and was performed according to the process available in the

[2] Supplementary data for this paper are available from the IUCr electronic archives (Reference: SN5001). Services for accessing these data are described at the back of the journal.

*JANA*2000 program (Petříček & Dušek, 2000). Table 5 gives the details on the orthogonalized function parameters.

### 3.2. Powder X-ray diffraction

Single crystals were crushed and ground to a fine powder with metallic lustre. The powder X-ray diffractogram contained, with the exception of a few very weak bumps, only one peak which was extensively broadened. As the single-crystal diffraction patterns showed no such contributions, it is obvious that the sample is very sensitive to grinding, indeed it seemed to go partially amorphous when subjected to mechanical treatment. As a reference, *ca* 50 approximately 0.05–0.1 mm large single crystals were mounted on sticky tape and measured with powder X-ray diffraction without any prior grinding. As expected, orientation effects when measuring on single crystals were visible in the powder diffractogram. Fig. 1 shows the powder diffractograms from the two measurements.

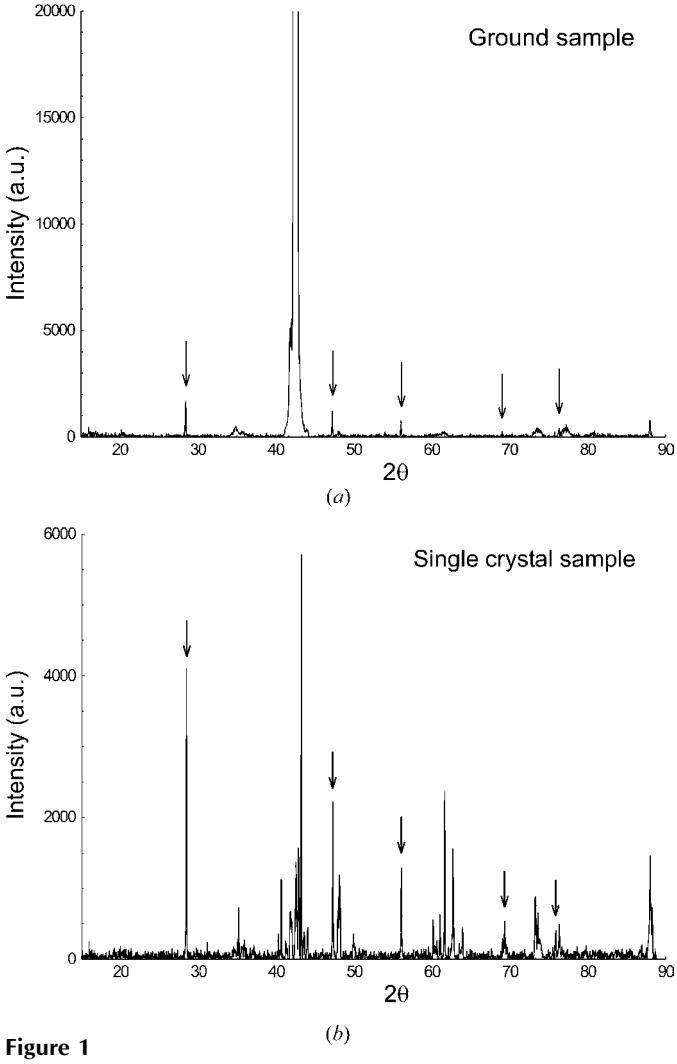


**Figure 1**
Powder diffractograms for (*a*) the ground sample and (*b*) the single-crystal sample. The peaks marked with arrows stem from silicon powder, which was used as an internal standard.

**Table 4**
Modulation function coefficients.

Modulation functions for a parameter λ of an atom ν defined in a restricted interval are defined by: $U^{\nu}_{\lambda}(\bar{x}_4) = \sum_{n=0}^{k} U^{\nu}_{\lambda,n}\mathrm{Ortho}^{\nu}_{n}(\bar{x}_4)$ where the orthogonalized functions, obtained through a Gram–Schmidt orthogonalization routine, are given by: $\mathrm{Ortho}^{\nu}_{i}(\bar{x}_4) = B^{\nu}_{0} + \sum_{n=1}^{k} A^{\nu}_{n}\sin(2\pi n\bar{x}_4) + \sum_{n=1}^{k} B^{\nu}_{n}\cos(2\pi n\bar{x}_4)$

| | |
|---|---|
| Positional parameters | |
| Co | $U^{c}_{x,1} = -0.0015$ (4), $U^{s}_{x,1} = 0.0010$ (3), $U^{c}_{y,1} = 0.003$ (2), $U^{s}_{y,1} = 0.001$ (7), $U^{c}_{z,1} = 0.0004$ (3), $U^{s}_{z,1} = 0.0027$ (3) |
| Zn1 | $U^{s}_{x,1} = 0.0113$ (2), $U^{c}_{y,1} = 0.016$ (4), $U^{s}_{z,1} = 0.00291$ (9) $U^{c}_{x,2} = -0.0031$ (2), $U^{s}_{y,2} = 0.004$ (2), $U^{c}_{z,2} = -0.0014$ (1) |
| Zn2 | $U^{s}_{x,1} = 0.0114$ (3), $U^{c}_{y,1} = 0.0153$ (3), $U^{s}_{z,1} = 0.0062$ (2) $U^{c}_{x,2} = -0.0017$ (3), $U^{s}_{y,2} = 0.0044$ (4), $U^{c}_{z,2} = -0.0015$ (2) |
| Zn3 | $U^{s}_{x,1} = -0.0047$ (2), $U^{c}_{y,1} = 0.0216$ (3), $U^{s}_{z,1} = 0.0025$ (2) $U^{c}_{x,2} = 0.0009$ (3), $U^{s}_{y,2} = -0.0044$ (5), $U^{c}_{z,2} = -0.0004$ (2) |
| Zn4 | $U^{s}_{x,1} = 0.0070$ (2), $U^{c}_{y,1} = -0.0309$ (3), $U^{s}_{z,1} = 0.00314$ (9) $U^{c}_{x,2} = -0.0012$ (2), $U^{s}_{y,2} = 0.0004$ (3), $U^{c}_{z,2} = 0.0012$ (2) $U^{s}_{x,3} = 0.0023$ (2), $U^{c}_{y,3} = 0.0085$ (3), $U^{s}_{z,3} = 0.0011$ (2) $U^{c}_{x,4} = 0.0005$ (3), $U^{s}_{y,4} = 0.0055$ (6), $U^{c}_{z,4} = -0.0005$ (3) |
| Zn5 | $U^{s}_{x,1} = 0.0090$ (2), $U^{c}_{y,1} = -0.0169$ (2), $U^{s}_{z,1} = -0.0174$ (2) $U^{c}_{x,2} = -0.0135$ (2), $U^{s}_{y,2} = 0.0081$ (3), $U^{c}_{z,2} = -0.0004$ (1) $U^{s}_{x,3} = -0.0035$ (2), $U^{c}_{y,3} = 0.0050$ (3), $U^{s}_{z,3} = 0.0012$ (2) $U^{c}_{x,4} = 0.0006$ (3), $U^{s}_{y,4} = -0.0015$ (6), $U^{c}_{z,4} = -0.0015$ (2) |
| Temperature parameters | |
| Zn1 | $U^{s}_{11,1} = 0.012$ (5), $U^{s}_{22,1} = 0.057$ (7), $U^{s}_{33,1} = 0.0015$ (6), $U^{c}_{12,1} = 0.062$ (4), $U^{s}_{13,1} = -0.0010$ (5) $U^{c}_{23,1} = -0.0009$ (4) |
| Zn2 | $U^{s}_{11,1} = 0.017$ (2), $U^{s}_{22,1} = -0.0008$ (8), $U^{s}_{33,1} = 0.0051$ (9), $U^{c}_{12,1} = -0.0024$ (6), $U^{s}_{13,1} = -0.0109$ (8) $U^{c}_{23,1} = 0.0008$ (5) |

## 4. Structure description

As a first step in the description of the features of the structure of $\delta_1$-$CoZn_{7.8}$, a commensurate approximation is used for reasons of clarity. In this approximation the structure can be illustrated as consisting of double icosahedra of Zn atoms, filled with Co atoms in both centres. The double icosahedra build up the entire structure by edge-sharing (edges between the apex atom and an atom in the nearest pentagonal layer) in the *c* direction and by face-sharing (faces between two pentagonal layers) in the *a* direction, *cf.* Fig. 2(*a*). In this manner, the building blocks are assembled so as to form helices along the unique *b* axis, *cf.* Figs. 2(*b*) and (*c*). The helices are then stacked together as in a distorted hexagonal packing and form the full structure drawn in Fig. 2(*d*). All helices are identical but are drawn differently in the figures, in order to clarify how the structure is built.

The structure can be considered as a close relative to the tetrahedrally close-packed structures (t.c.p.), which are constituted only by tetrahedral interstices. The single polyhedron that separates the structure from a t.c.p. structure is an octahedron, situated in the void between the pentagonal channels (the helices) in the title structure. The octahedron is surrounded by severely tilted empty tetraedersterns (Hyde & Andersson, 1989). In the *ac* plane, reference can be made to the t.c.p. structure of $Zr_4Al_3$ (Wilson *et al.*, 1960), which is built up by straight tetraedersterns that create linear pentagonal antiprismatic channels along the [110] direction. The channels are juxtapositioned in the same manner as in the title structure, *cf.* the section marked with dotted lines in Fig. 2(*a*).

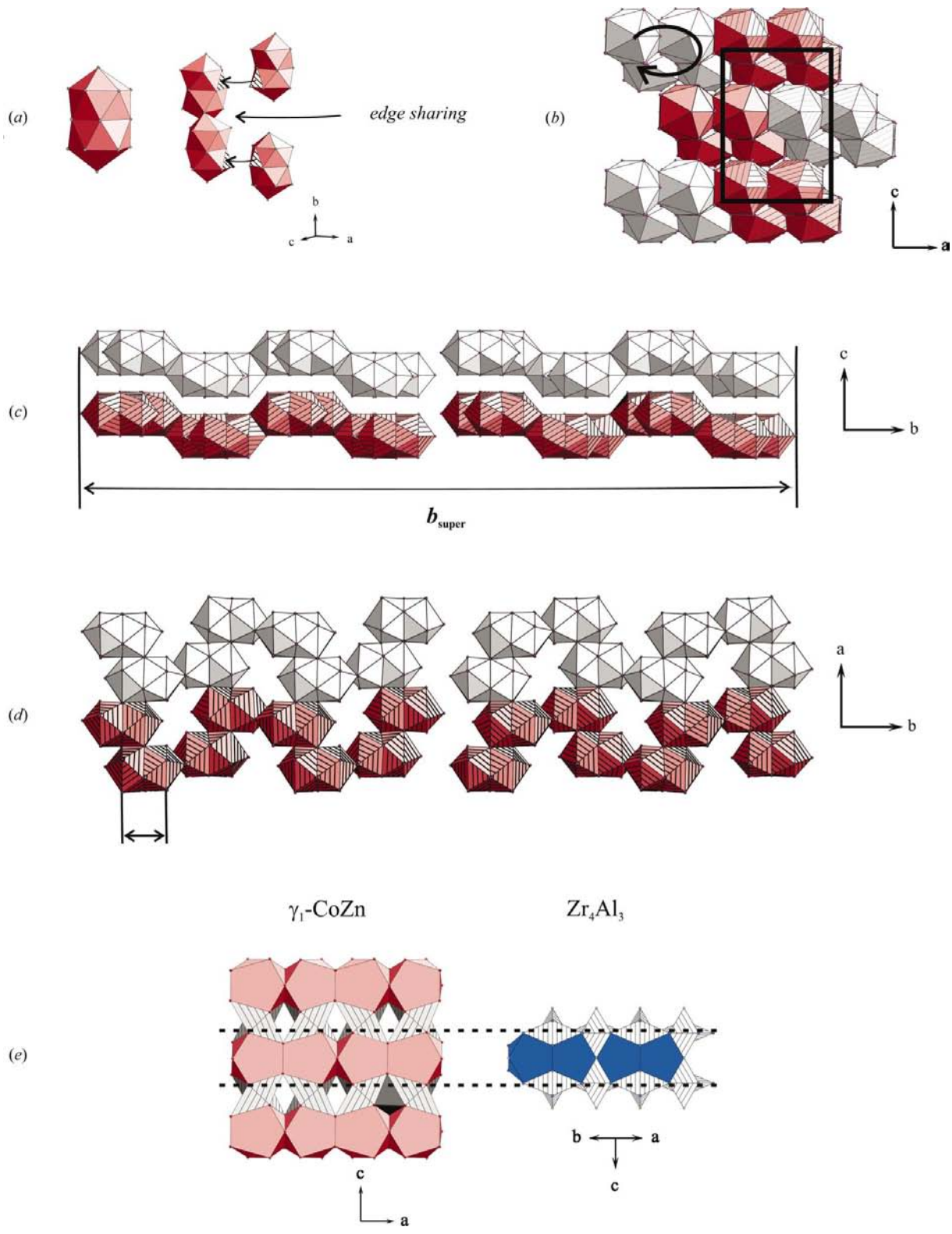


**Figure 2**
(*a*) The double icosahedron to the left with cobalt in the centres of the pentagonal antiprisms. The right picture illustrates how the icosahedra are assembled with edge and face sharing. (*b*) The commensurate approximation viewed along the *a* direction, where the icosahedra share faces. This approximation corresponds to a 73.7 Å large $b_{super}$ cell, indicated in the picture. (*c*) The commensurate supercell viewed along the *c* direction, where the icosahedra share edges. The *b* cell parameter of the incommensurate structure is marked in the picture by arrows. (*d*) The structure forms helices along the *b* direction. Different colours are used to clarify the separate (but identical) helices. The black box refers to the unit cell and the curved arrow refers to the helix rotation direction. (*e*) Comparison between the title structure to the left and the $Zr_4Al_3$ structure to the right. The empty space between the helices in the title structure clearly visible in (*b*) can be described as tilted tetraedersterns, marked with broken lines, whereas in the $Zr_4Al_3$ structure the tetraedersterns are straight. The positioning of the pentagonal channels is equivalent in both structures, this section is indicated with dotted lines. The polyhedron marked in darker grey in the $\delta_1$ structure is an octahedron.

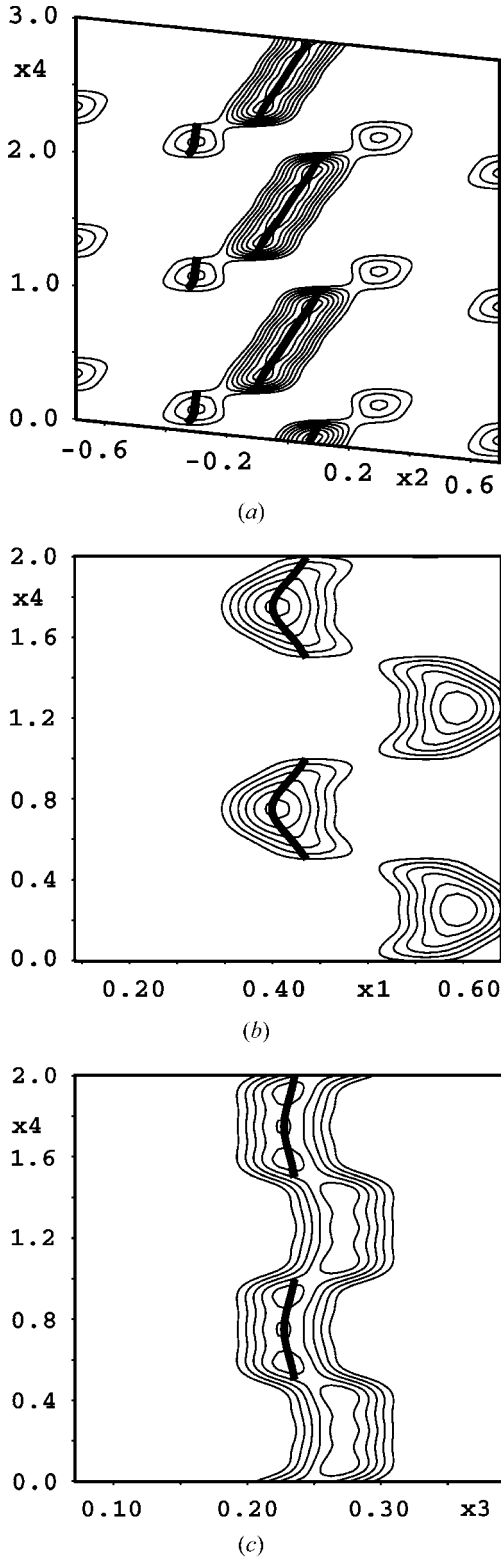


**Figure 3**
Sections of the electron density maps calculated from $F_{obs}$. (*a*) Modulation functions of the Zn1 and Co atoms along *b* ($x1 = -0.213$ and $x3 = 0.091$), a typical form of a sawtooth function. The refined AMFs are indicated by the heavy line (Zn1) and the dotted line (Co). (*b*) AMF of Zn2 along *b*, section taken at $x3 = -0.002$ and $x2 = 0$. The heavy line indicates the refined position. (*c*) AMF of Zn3 along *b*, section taken at $x3 = 0.248$ and $x2 = 0$. The heavy line indicates the refined position.

**Table 5**
Orthogonalized function parameters.

| $\text{Ortho}_i^{\text{Co}}$ | $B_0$ | $A_1$ | $B_2$ |
|---|---|---|---|
| $i = 0$ | 1 | | |
| $i = 1$ | −3.322 | 4.323 | |
| $i = 2$ | −20.803 | 31.365 | 11.454 |

| $\text{Ortho}_i^{\text{Zn1}}$ | $B_0$ | $A_1$ | $B_1$ | $A_2$ | $B_2$ |
|---|---|---|---|---|---|
| $i = 0$ | 1 | | | | |
| $i = 1$ | 0.497 | 1.774 | | | |
| $i = 2$ | 0 | 0 | 1.287 | | |
| $i = 3$ | 0 | 0 | 0.199 | 1.417 | |
| $i = 4$ | −0.870 | −1.611 | 0 | 0 | 2.020 |

| $\text{Ortho}_i^{\text{Zn2}}$, $\text{Ortho}_i^{\text{Zn3}}$ | $B_0$ | $A_1$ | $B_1$ | $A_2$ | $A_3$ |
|---|---|---|---|---|---|
| $i = 0$ | 1 | | | | |
| $i = 1$ | 2.069 | 3.249 | | | |
| $i = 2$ | 0 | 0 | 1.414 | | |
| $i = 3$ | 0 | 0 | 2.271 | 2.675 | |
| $i = 4$ | 2.187 | 2.785 | 0 | 0 | 1.973 |

The most reasonable commensurate approximation to the incommensurate $\delta_1$ structure is a 17-fold superstructure along the unique axis. This is the result of an approximation of the measured $\mathbf{q} \simeq 0.234$ [010]* to $\mathbf{q} = 4/17$ [010]* and will in a three-dimensional structure description produce a *b* axis of 73.7 Å (see Figs. 2*b* and *c*) and the space group $F\bar{1}$. The *b* cell parameter of the incommensurate structure corresponds to two average interplanar spacings. Besides the large difference in cell volume between any commensurate approximation and the incommensurate structure model, the main difference lies in the description of the Co atoms in the latter model as guests in the t.c.p. host lattice. The structural modulation reveals itself as changes in the number of fused icosahedra, causing occasional occurrences of single or triple icosahedra.

Electron density maps of the atomic positions show that Zn1 has the greatest deviation from the average position. This Zn atom is located at the apex of the double icosahedron. Fig. 3(*a*) shows the $x_2$–$x_4$ projection of the sawtooth functions applied to the cobalt and Zn1 atoms, illustrating the large movement of the Zn1 atom. In order to model the deviations of the Co and Zn1 atoms from their average positions in the *ac* plane, harmonic positional displacement waves were applied together with the sawtooth functions. These, and all other displacement waves applied on the atoms, gave small deviations from the average positions. The Zn2 and Zn3 atoms were modelled with crenel functions in order to describe the positional leap from one icosahedron to another as the helix turns around, *cf.* Figs. 3(*b*) and (*c*). Fig. 4 presents the modulation function behaviour for all atoms.

The interatomic distances in modulated structures often vary substantially, as the distances between atoms clearly depend on the deviations of the atomic positions. The Co—Co distances in the title structure range from 2.6 to 2.7 Å, the Co—Zn distances from 2.5 to 3.2 Å and the Zn—Zn distances from 2.44 Å upwards. The heteroatomic distances can thus not be distinguished in length from the homoatomic distances, an

observation in agreement with the other icosahedrally built cobalt–zinc compounds.

Neither the scattering factors nor the interatomic distances change significantly when zinc is replaced by cobalt. Regardless of this, two signs strongly indicate the position of the Co atom. The first indication stems from the icosahedral coordination typical for transition metals in zinc-rich compounds and the second indication is the previously mentioned fact that the cobalt amount determined by EDX is in excellent agreement (less than 0.1% difference) with the results of $\Delta_{Co}$ (the width of the sawtooth function for Co, as explained above) from the refinement, when no restrictions on the width were applied.

## 5. Discussion

### 5.1. Geometrical considerations

The high abundance of icosahedra in the cobalt–zinc system may be rationalized from the relation between the radii of the elements and the properties of the regular icosahedron. The metallic radius of cobalt is 1.25 Å, while the metallic radius of zinc is 1.34 Å. If Zn atoms are placed on the vertices of an icosahedron and a Co atom is placed in the centre, the combined radii of the elements result in the distance between a vertex and the centre being 0.966 of the distance between adjacent vertices. In a regular icosahedron the vertex-to-centre distance is 0.951 of the vertex-to-vertex distance (*cf. Appendix A*), hence proving that zinc and cobalt fit very well into an icosahedral packing.

In a chain of interpenetrating icosahedra (a sequence of pentagonal antiprisms), the distance between the centres is $\tau/(\tau+2)^{1/2}$ or approximately 0.851 of the vertex-to-vertex distance (*cf. Appendix A*), an important difference of 10% from the vertex-to-centre distance. This applies an additional and incompatible demand on the radii relation of the elements of the structure. Regardless of this, nature does present several examples in violation of the simple geometrics stated above. The examples can be divided into groups according to their different solutions, as follows:

(i) Structures with a rigid icosahedral shell of a single atomic element that consequently, owing to the underlying icosahedral geometry, force the centre atoms to extremely short distances. This occurs in the series of tantalum-rich sulfides with all-tantalum pentagonal antiprisms (first reported by Franzen & Smeggil, 1969, 1970) and in the related tantalum (or mixed Ta, Nb) chalcogenides (Debus & Harbrecht, 2002, and references therein). The constant but short centre-to-centre distances are typical for these compounds. In the $A_5Cd_2Tl_{11}$ ($A$ = Cs, Rb) compounds (Kaskel & Corbett, 2000), the centre Cd atoms are forced to form pairs, both centre-to-centre distances being unusually short.

(ii) If, on the other hand, the centre atoms are well distributed in an ordered manner and with reasonable distances in-between, the antiprismatic shell is subject to distortion and often constituted by two or more elements. Examples are the $\mu$ phase (Forsyth & d'Alte da Veiga, 1962), the $Zr_4Al_3$ structure (Wilson *et al.*, 1960) and the $\tau$-$Al_{2.9}Ta_{2.7}V_{1.4}$ structure (Harbrecht *et al.*, 1996).

(iii) The structure of $Al_5Fe_2$ (Burkhardt *et al.*, 1994) gives a disordered solution to the geometric problem, as the centre Al atoms are poorly localized in the mixed pentagonal antiprismatic shell.

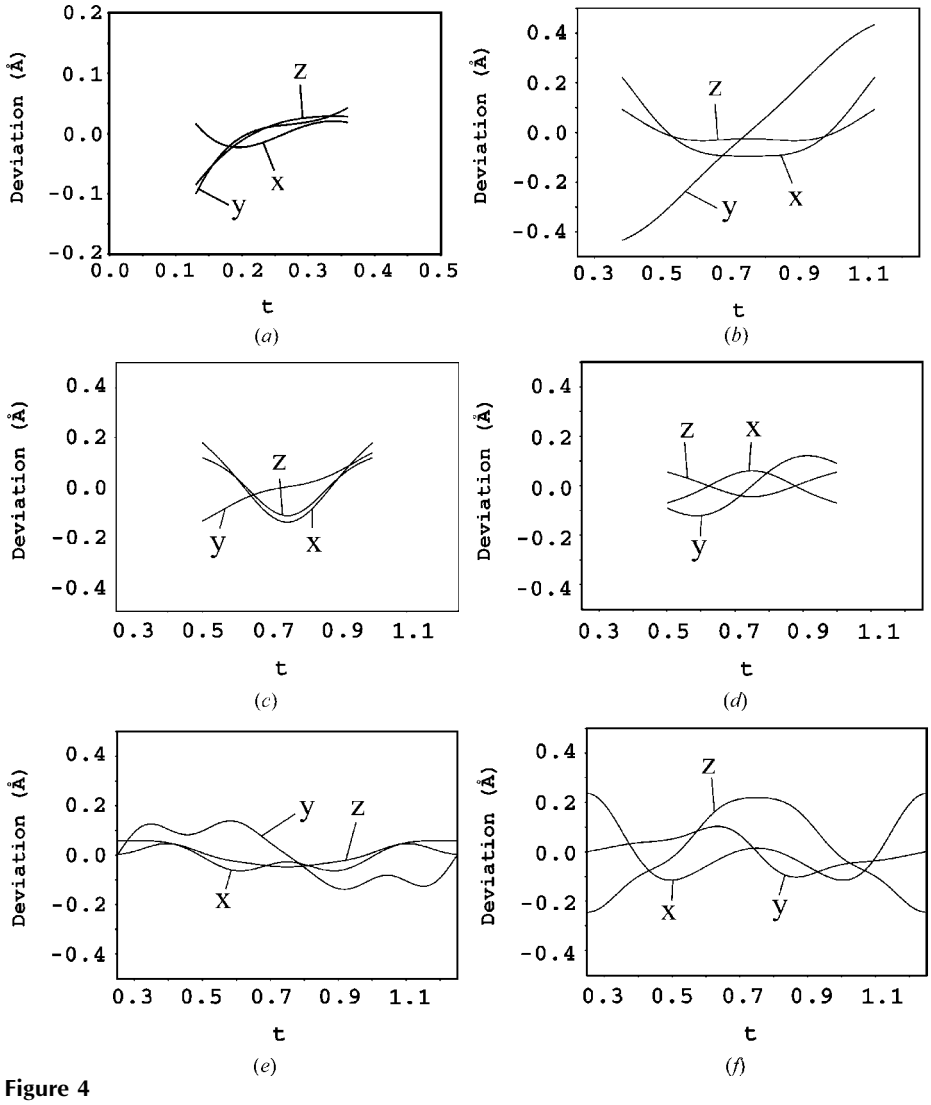


**Figure 4**
Refined modulation functions along the $x$, $y$ and $z$ directions, shown as $t$ plots for (*a*) Co, (*b*) Zn1, (*c*) Zn2, (*d*) Zn3, (*e*) Zn4 and (*f*) Zn5.

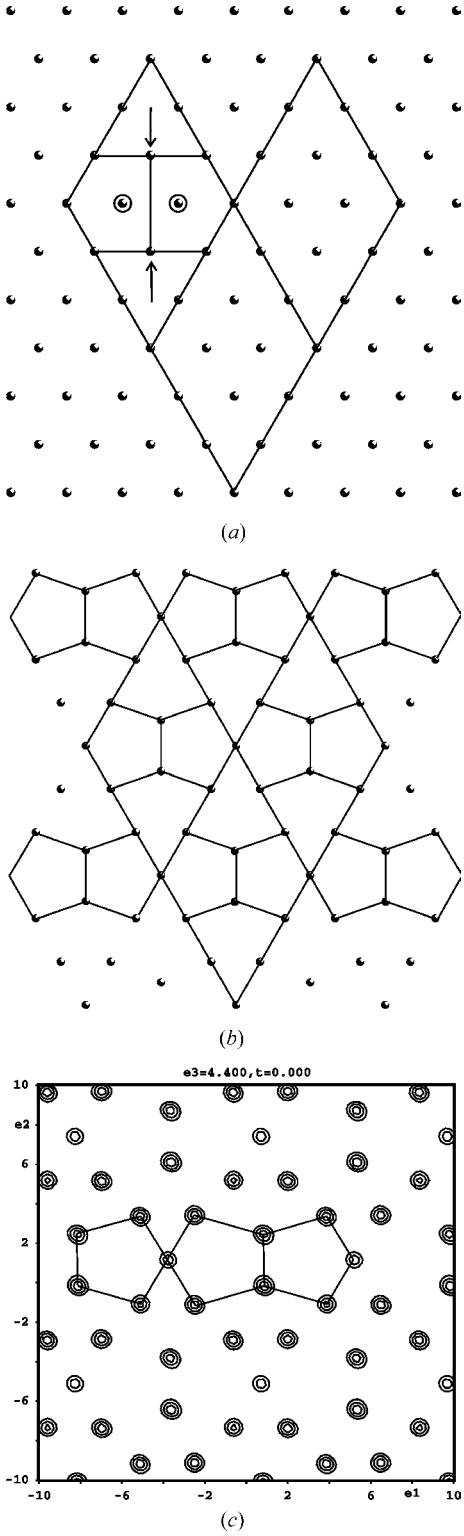


**Figure 5**
The construction of a pentagonal layer from a hexagonal close packing. (*a*) If the atoms surrounded by circles are subtracted in an arbitrary $3 \times 3$ supercell, the neighbouring atoms and especially those marked with arrows will relocate in compensation for the larger space. With this change pentagons are created in the initial lattice, as shown in (*b*), which is much similar to a pentagonal layer in the title structure, shown in (*c*). If the subtracted atoms are repositioned into the next layer, between the hexagonal close-packed layers, and are set to be Co atoms and the atoms constituting the pentagonal net are Zn atoms, we have constructed pentagonal antiprismatic channels of zinc filled with Co atoms.

The $\delta_1$-$CoZn_{7.8}$ structure is perhaps best identified as a member of the last group, as the centre atomic position is disordered with respect to the shell since it has a periodical deviation of the average centre position. However, where in the $Al_5Fe_2$ structure the disordered centre atoms continue linearly along the columns, the corresponding pentagonal 'columns' in the title structure are strikingly short. The linear sequence of centre atoms breaks after no more than a few atoms and continues in another segment. Although the fused icosahedra have distorted shells and the cobalt–cobalt distances are shorter than in cobalt metal, these adjustments are not enough to build a linear pentagonal column. The distance between two Co atoms in a metal is 0.93 of that between two Zn atoms in a metal, a fact that restricts the conditions for a pentagonal antiprismatic sequence of zinc and cobalt radically in the sense that the cobalt–zinc distances limit the chain to no longer than two overlapping icosahedra (a double icosahedron). A third attached icosahedron would strain the cobalt–zinc bonds to intolerably short distances, even when adjustments are made in both shell and centre-to-centre contacts. In this system, a linear sequence of interpenetrating icosahedra is thus confined to double icosahedra, from the single justification of considering the radii relation of the elements.

As stated above, the $\delta_1$-$CoZn_{7.8}$ structure is closely related to the t.c.p. structures. In fact, there is a simplistic way to convert a $3^6$ net into the pentagon-net upon which the title structure is based. By the removal of two nodes out of nine in a $3 \times 3$ supercell, and allowing the remaining nodes to relax according to Figs. 5(*a*) and (*b*), a net much resembling that formed by the Zn atoms in the title compound is formed. Moreover, if the missing nodes are simply displaced out of the plane of the net, they nicely mimic the positions of the Co atoms in the centres of the pentagonal antiprisms or the apex Zn1 atoms. The absolute location of displaced nodes with respect to the $3 \times 3$ supercell in the $3^6$ net is naturally arbitrary and an identical pattern, differing only in absolute location with respect to the origin of the original $3^6$ net, may be generated by a different choice. It is thus simple to visualize how the re-entry of the displaced nodes into the plane and the subsequent displacement of a new set of nodes will appear as the complete motion of the entire motif. In the sequence of Fig. 6(*a*)–(*e*) such a mechanism is shown. In Fig. 6(*a*) the pentagonal pattern is intact and the displaced nodes (Zn1 atoms) are well out of the plane of the net. In Fig. 6(*b*) the displaced nodes have started their re-entry and in Fig. 6(*c*) the re-entry is complete, leading to a large-scale in-plane motion of one of the neighbouring nodes and subsequently to an out-of-the-plane removal of a next-nearest neighbour (Fig. 6*d*). The final result is the shift of the entire net shown in Fig. 6(*e*).

### 5.2. The modulation mechanism

Considering that the Co atom is a little too large to fit in an extended pentagonal antiprismatic column, the mechanism provides a relaxation pathway for the structure. As the Co atom progresses closer to the Zn net, this net responds by

reorganization and expulsion of a next-nearest neighbour atom that forms the centre of the new pentagonal antiprismatic column. The behaviour of the layer is reminiscent of how billiard balls behave if forced into too narrow a frame; one ball will stay on top. If this ball is forced down, another one pops up. Again it must be stressed that the choice of atomic species Co/Zn is based on the similarity with other structures and compositional considerations only. It was not possible to distinguish between the two from X-ray scattering data.

The incommensurability of the structure may be understood from the same mechanism; the whole strain-driven process propagates along the unique axis in a continuous process. The re-entry of the displaced node into the plane pushes the next-nearest neighbour node out of the plane, locally relaxing the strain, but simultaneously nucleating a new source of strain in the new pentagonal antiprismatic column. Moreover, the position of the new out-of-the-plane node is slightly different from the corresponding node in the preceding column and this secondary strain will slowly build up over a longer distance, occasionally being relieved as a single or triple pentagonal antiprism.

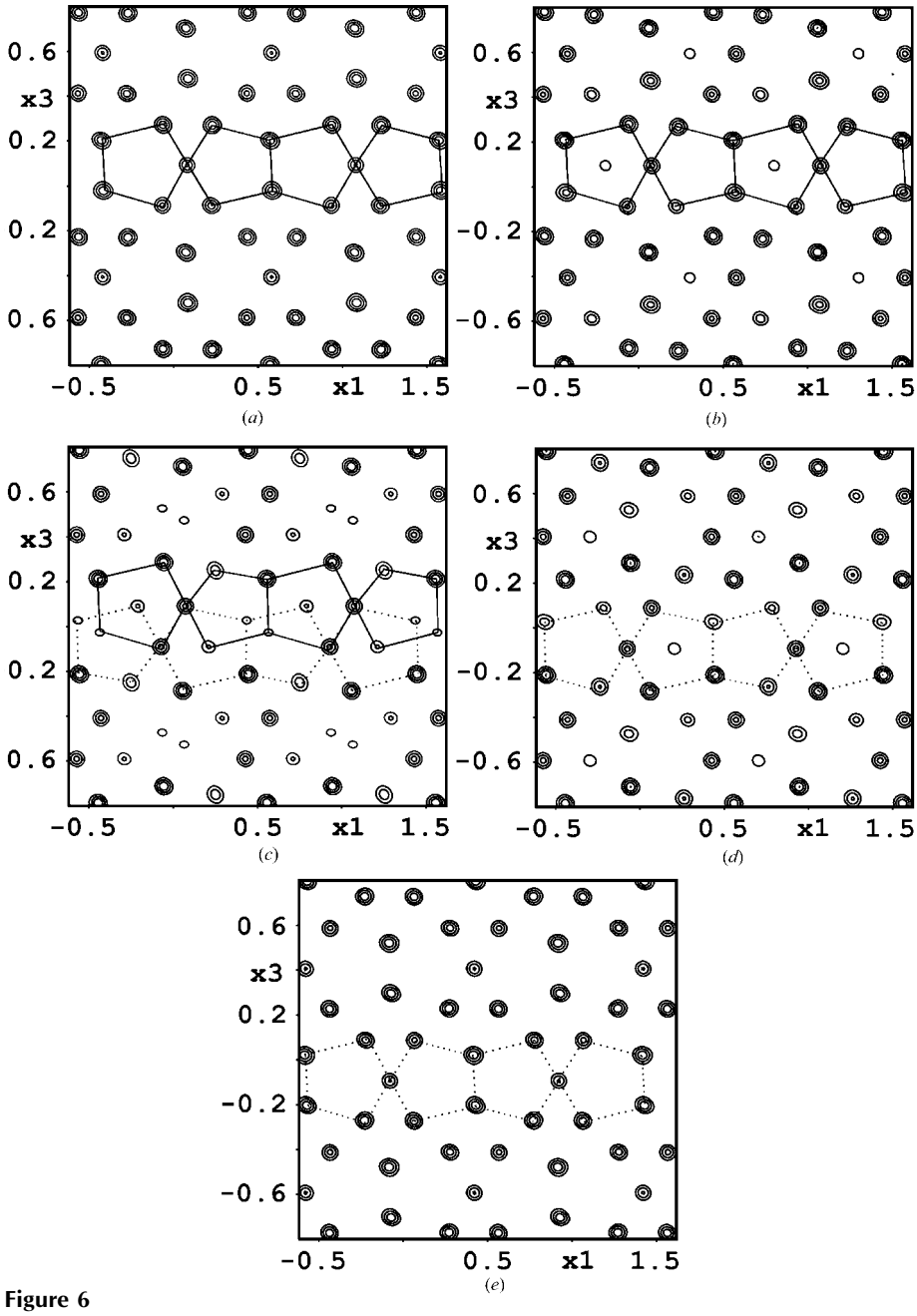


**Figure 6**
Pentagonal layers in the $\delta_1$-$CoZn_{7.8}$ structure shown as $x_1$–$x_3$ graphs illustrating the positional changes of the atoms along the modulational direction [010]. (*a*) shows a layer at $x4 = 0.38$, with Zn atoms as they appear when forming pentagons in the double icosahedron. The Zn1 atom starts to appear in (*b*) in the centre of a pentagon as the double icosahedron is about to close (at $x4 = 0.44$). In (*c*) the cell shift is being realised ($x4 = 0.50$) and in (*d*) at $x4 = 0.53$, the cell has been shifted and another double icosahedron grows up with a layer of pentagons in (*e*) at $x4 = 0.62$. The co-existence of two small electron density peaks in (*c*) is a drawback of the Fourier function modelling. The 'tail' of this function does not vanish as fast as the electron density does, resulting in two apparent atoms in the map although of course only one is present.

## 6. Conclusions and future directions

The structure of $\delta_1$-$CoZn_{7.8}$ displays features that are reminiscent of phasons frozen in space. This would imply that a high-temperature modification of the phase might display phason dynamics. A phase transformation to this disordered state would be manifested both in the loss of superstructure ordering and a widening of the Bragg peaks of the main structure. Since the transformation would be second order, it may be difficult to detect it by thermal methods. The X-ray scattering characteristics of such a phason pinning–unpinning transformation are in fact exhibited by the sample after grinding. This would indicate that the ordered structure is in fact metastable at room temperature and that the mechanical energy is enough to trigger the transformation.

Conclusive proof that this transformation can be accomplished thermally requires high-temperature diffraction experiments. We are now in the process of setting up such an experiment.

## APPENDIX *A*

An ideal icosahedron with edge length 2 is inscribed in a cube (Fig. 7*a*). The vertex positions are given by

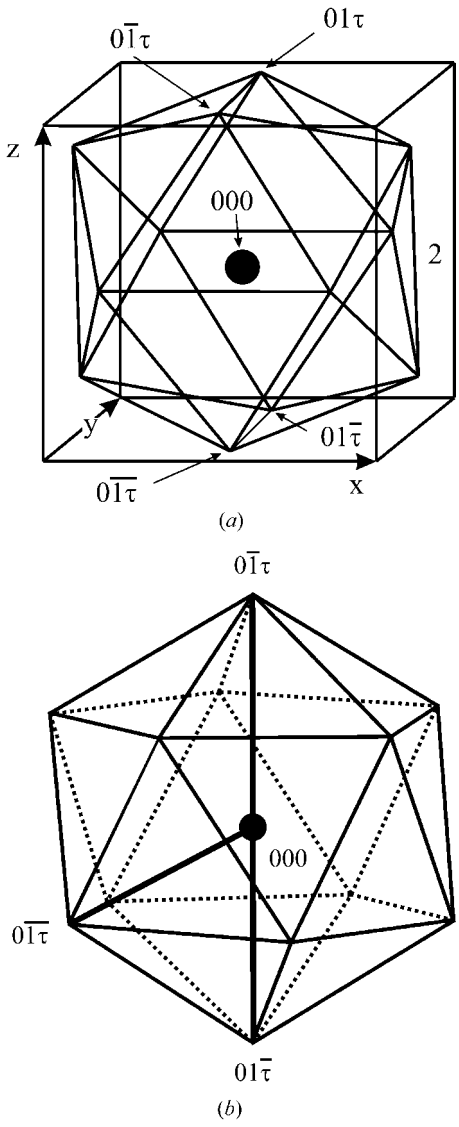


**Figure 7**
(*a*) An ideal icosahedron placed inside a cube. (*b*) Half of the distance between two parallel pentagons is the length of the vector **u** projected on **v**.

the even permutations of $(0\ \pm1\ \pm\tau)$. The vertex-to-centre distance is then $|01\tau| = (1+\tau^2)^{1/2}$. The ratio between this length and the edge length is $\simeq 0.951$. The longest diagonal in the icosahedron is the vector $v = (0\bar{1}\tau) + (01\bar{\tau}) = 2(0\bar{1}\tau)$, see Fig. 7(*b*). Half of the distance between two parallel pentagons is the length of the vector $\mathbf{u} = (01\tau)$ projected on $\mathbf{v}$, $\mathbf{u}\cdot\mathbf{v}/|\mathbf{v}| = \tau^2 - 1/(\tau^2+1)^{1/2}$. Given that $\tau^2 = 1+\tau$ this simplifies to $\tau/(\tau+2)^{1/2}$. The ratio between the height of the pentagonal antiprism and the edgelength is thus $\sim$0.8506.

This work was financially supported by the Swedish Natural Science Research Council, the Swedish Foundation for Strategic Research and the Grant Agency of the Czech Republic (grant No. 202/03/0430). M. Dzugotov is acknowledged for valuable discussions.

## References

Boström, M. & Hovmöller, S. (2000). *J. Solid State Chem.* **153**, 398–403.
Boström, M. & Lidin, S. (2002). *J. Solid State Chem.* **166**, 53–57.
Brown, P. J. (1962). *Acta Cryst.* **15**, 608–612.
Burkhardt, U., Grin, Yu. & Ellner, M. (1994). *Acta Cryst.* B**50**, 313–316.
Debus, S. & Harbrecht, B. (2000). *Z. Anorg. Allg. Chem.* **626**, 173–179.
Ekman, Z. (1931). *Phys. Chem.* **12**, 57–78.
Forsyth, J. B. & d'Alte da Veiga, L. M. (1962). *Acta Cryst.* **15**, 543–547.
Franzen, H. F. & Smeggil, J. G. (1969). *Acta Cryst.* B**25**, 1736–1741.
Franzen, H. F. & Smeggil, J. G. (1970). *Acta Cryst.* B**26**, 125–129.
Harbrecht, B., Rheindorf, N. & Wagner, V. (1996). *J. Alloys Compd*, **234**, 6–11.
Hyde, B. G. & Andersson, S. (1989). *Inorganic Crystal Structures*. New York: John Wiley & Sons.
Kaskel, S. & Corbett, J. D. (2000). *Inorg. Chem.* **39**, 3086–3091.
Massalski, T.B. (1990). Editor. *Binary Alloy Phase Diagrams.*, 2nd ed. ASM International, USA.
Petříček, V. & Dušek, M. (2000). *JANA*2000. Institute of Physics, Praha, Czech Republic.
Petříček, V., van der Lee, A. & Evain, M. (1995). *Acta Cryst.* A**51**, 529–535.
Schramm, J. (1938*a*). *Z. Metallkdd.* **30**, 10–14.
Schramm, J. (1938*b*). *Z. Metallkdd.* **30**, 122–130.
Sheldrick, G. M. (1997). *SHELXS*97. University of Göttingen, Germany.
Stoe & Cie (1996*a*). *XRED*. Stoe & Cie, Darmstadt, Germany.
Stoe & Cie (1996*b*). *XSHAPE*. Stoe & Cie, Darmstadt, Germany.
Wilson, C. G., Thomas, D. K. & Spooner, F. J. (1960). *Acta Cryst.* **13**, 56–57.